Phase Segregation in Polystyrene–Polylactide Blends

ARTICLE *in* MACROMOLECULES · MARCH 2009

Impact Factor: 5.8 · DOI: 10.1021/ma802176b

Phase Segregation in Polystyrene−Polylactide Blends

Bonnie O. Leung,[†] Adam P. Hitchcock,*[,†] John L. Brash,[‡] Andreas Scholl,[§] and Andrew Doran[§]

BIMR, McMaster University, Hamilton, ON, Canada L8S 4M1; School of Biomedical Engineering, McMaster University, Hamilton, ON, Canada L8S 4M1; and Advanced Light Source, Berkeley Laboratory, Berkeley, California 94720

Received September 25, 2008; Revised Manuscript Received January 13, 2009

ABSTRACT: Spun-cast films of polystyrene (PS) blended with polylactide (PLA) were visualized and characterized using atomic force microscopy (AFM) and synchrotron-based X-ray photoemission electron microscopy (X-PEEM). The composition of the two polymers in these systems was determined by quantitative chemical analysis of near-edge X-ray absorption signals recorded with X-PEEM. The surface morphology depends on the ratio of the two components, the total polymer concentration, and the temperature of vacuum annealing. For most of the blends examined, PS is the continuous phase with PLA existing in discrete domains or segregated to the air−polymer interface. Phase segregation was improved with further annealing. A phase inversion occurred when films of a 40:60 PS:PLA blend (0.7 wt % loading) were annealed above the glass transition temperature (T_g) of PLA.

1. Introduction

Polylactide (PLA) or poly(lactic acid) is studied extensively since it is valuable in biomedical and pharmaceutical applications due to its biodegradable and biocompatible nature.[1−3] However, the brittleness of PLA impedes its development for large-scale commercial use.[4] Thus, PLA has been blended with a variety of materials such as natural fibers,[5,6] plasticizers,[7] and synthetic, nonbiodedgradable polymers to enhance physical properties such as elasticity[8] and tensile strength.[9] In particular, PLA combined with polystyrene (PS) has been investigated as a potential bioblend with proposed applications in materials packaging and tissue engineering.[10]

PS−PLA block copolymers have recently been found to exhibit a rich variety of nanopatterns such as cylinders[11−13] and cocontinuous structures[14] which form during phase segregation of PS and PLA and arise from the immiscibility of the two polymers.[15] Selective removal of either component gives rise to ordered nanochannels suitable as catalytic supports or scaffolds in tissue engineering. Improving the physical properties of these materials depends on control of the interface between the two polymers which controls its microstructure.[14] Thus, characterization of the morphology of PS-*b*-PLA block copolymers, as well as PS−PLA blends, remains key in the development of novel, high-performance, PS−PLA-based materials.

We are using soft X-ray spectromicroscopy to study phase segregation in spun-cast thin films of PS−PLA blends. Our techniques provide quantitative information on the composition of these polymers. Several studies have utilized near-edge X-ray absorption fine structure (NEXAFS) spectra obtained in an X-ray photoemission electron microscope (X-PEEM) or scanning transmission X-ray microscope (STXM) to characterize immiscible polymer blends.[16−21] Our research group has previously used X-PEEM to characterize spun-cast films of phase-segregated polystyrene (PS)−poly(methyl methacrylate) (PMMA) with respect to polymer molecular weights and annealing times and temperatures.[22] The chemical sensitivity, particularly at the C 1s edge, combined with the near-surface sensitivity of X-PEEM, provides quantitative characterization of the composition and morphology in the outermost ∼10 nm of the film.

* Corresponding author. E-mail: aph@mcmaster.ca.
[†] BIMR, McMaster University.
[‡] School of Biomedical Engineering, McMaster University.
[§] Berkeley Laboratory.

The aim of this work is to visualize and quantitatively analyze different morphologies produced at the surfaces of PS−PLA films by varying mass ratio, total polymer concentration, and annealing times. This study is part of an effort to develop phase-segregated PS−PLA films with surface microstructure in the submicron range as candidate semibiodegradable biomaterials. A subsequent paper will report our investigations of protein adsorption on the more promising PS−PLA substrates.[23]

2. Materials and Methods

2.1. Materials. Polystyrene (MW = 104K, δ = 1.05) and polylactide (MW = 33K, δ = 1.33) were obtained from Polymer Source Inc. and used as received. The samples were of high purity, as confirmed by proton NMR. Varying ratios of the two polymers were spun-cast (4000 rpm, 40 s) from 1.0, 0.7, and 0.4 wt % dichloromethane solutions onto clean 1 × 1 cm native oxide silicon wafers (Wafer World, Inc.) and degreased with trichloroethylene, acetone, and methanol, followed by rinsing with doubly deionized water. The PS−PLA substrates were annealed at 45 °C (1 and 6 h) and 70 °C (1 h) in a vacuum oven at a pressure $\sim 10^{-5}$ Torr, achieved with a cryo-trapped turbo pump.

2.2. Atomic Force Microscopy (AFM). AFM images were collected with a Quesant Q-scope 250 (Quesant Instruments, Ambios Technology, Santa Cruz, CA), operated in noncontact mode. Standard noncontact silicon cantilevers from Quesant were used. Phase and height mode images (10 × 10 μm) were collected simultaneously at a scan rate of 1.8−2.0 Hz under ambient conditions.

2.3. STXM. A scanning transmission X-ray microscope (STXM) was used to collect high-quality reference spectra of PS and PLA. The STXM operates in transmission mode and offers slightly better energy resolution (0.1−0.2 eV) compared to X-PEEM (0.4−0.5 eV); however, similar NEXAFS line shapes are obtained from both methods. The STXM data were collected on beamline 5.3.2 at the Advanced Light Source (ALS) in Berkeley, CA.[24,25] Typically, solvent-cast samples with thickness below 100 nm were analyzed by collecting micrometer-sized stacks. Image sequences[26] were used in homogeneous areas to minimize radiation damage. An image at a damage-sensitive energy (288.5 eV)[27] was recorded after each spectral measurement to monitor damage. Only results from measurements with negligible (<10%) damage were used analytically.

2.4. X-PEEM. All X-PEEM measurements were performed at the ALS on the PEEM-2 instrument on beamline 7.3.1 using elliptical right circularly polarized light (70−80%). Detailed accounts of the experimental apparatus, beamline setup, and

10.1021/ma802176b CCC: $40.75
Published on Web 02/16/2009

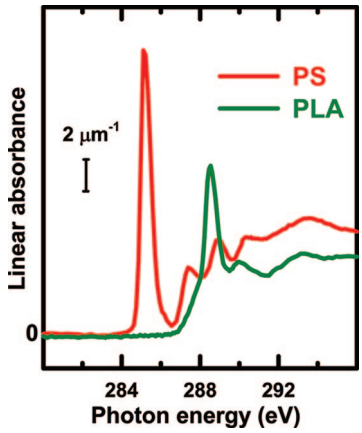

Figure 1. C 1s X-ray absorption spectra of polystyrene (PS, red) and polylactide (PLA, green), as recorded in STXM. The spectra are plotted on an absolute linear absorbance scale, after subtraction of a linear background to isolate only the C 1s signal.

instrument optics have been presented previously.[28] In short, photoelectrons and secondary electrons ejected by absorption of the monochromatic X-rays are accelerated into an electrostatic imaging column, where the spatial distribution is magnified and detected by a CCD camera. X-PEEM is a surface-sensitive technique with a sampling depth (1/e) of 4 nm for polymers,[29] with the integrated signal sampling the top 10 nm of the sample.

A 100 nm thick Ti foil was used as a second-order light filter. To minimize radiation damage, a fast shutter (0.1 s) was used. This reduced the X-ray exposure by 50% by blocking the beam during the time required to transfer images from the CCD camera and to step the photon energy. The incident flux was reduced to about 10% of the full intensity by masking the beam upstream of the monochromator. A limited number of energies (23 in C 1s) and a short exposure time (1 s) per image were used as other ways to minimize radiation damage. The field of view was approximately 20 × 20 μm.

2.5. X-PEEM Chemical Mapping and Quantitative Analysis. The reference C 1s spectra for PS and PLA are presented in Figure 1 on a quantitative linear absorbance scale. The two species are easily differentiable. PS is characterized by an intense C 1s → $\pi^*_{C=C}$ transition at 285.15(3) eV while PLA exhibits a strong C 1s → $\pi^*_{C=O}$ transition at 288.53(3) eV.

All quantitative analyses were performed with the aXis2000 software package.[30] The C 1s image sequences were aligned (if needed), normalized to the ring current, and divided by the I_0 spectrum obtained from a clean HF-etched Si(111) chip. Next, the spectrum was corrected for the absorption of Si with a linear energy term representing the bolometric response of PEEM detection. Each stack was calibrated by assigning the peak of the C 1s → $\pi^*_{C=C}$ transition of PS to 285.15 eV.

The spectrum at each pixel was fit to linear combinations of the PS and PLA reference spectra using singular value decomposition (SVD), which provides an optimal solution for the analysis of highly overdetermined data sets.[31,32] The fit coefficients at each pixel provide component maps which are the spatial distribution of each component (Figure 2). Nonuniform illumination was corrected by dividing each component map by a heavily smoothed version of the sum of all component maps. Since X-PEEM samples ~10 nm into the surface, the intensity scale of the sum of the component maps was set to 10 in order to give estimates of the thickness in nanometers of each component in the sampled region.[29]

Next, a threshold mask was applied to the PS and PLA component maps to identify those pixels corresponding to PS-rich or PLA-rich areas (Figure 3a,b). Threshold levels were adjusted manually to a value which isolated only the domains of common spectral characteristics as determined by the color-coded composite maps. The average spectra extracted from the PS-rich and PLA-rich regions were further modified by setting the pre-edge region

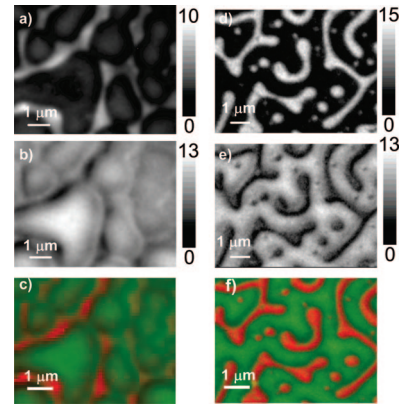

Figure 2. (left) Component maps of (a) PS and (b) PLA, derived from C 1s image sequences measured from an as-spun 40:60 PS:PLA (1 wt %) film (gray scale is thickness in nanometers). (c) Rescaled color composite map (red = PS, green = PLA). (right) Component maps of (d) PS and (e) PLA, derived from C 1s image sequences measured from 40:60 PS:PLA (0.7 wt %) film annealed 1 h at 70 C. (f) Rescaled color composite map. In (c) and (f), the relative contribution from red has been increased by 40% and that of green has been decreased by 20% in order to visualize more clearly the continuous domain, which is PS-rich in (c) and PLA-rich in (f).

to zero intensity, followed by least-squares fit to the same PS and PLA reference spectra used to generate the component maps (Figure 3c,d). Several stacks were obtained for each sample and the compositional results from these independent repeat measurements were averaged to yield the final quantitative results. The uncertainties cited in Table 1 are the standard deviations from these multiple determinations.

3. Results

3.1. Optimization of a PS−PLA Blend System. *3.1.1. Polymer Weight Ratios.* Four solutions with PS:PLA w/w ratios of 20:80, 40:60, 60:40, and 80:20 (1% total polymer weight) were dissolved in dichloromethane and spun-cast on Si(111). The AFM phase mode micrographs of these samples are displayed in Figure 4a−d. AFM revealed interesting variations in the microstructure at the surface, particularly for the 40:60 and 60:40 PS:PLA ratios. Although AFM provides excellent height resolution at the surface (<1 nm), it does not have any intrinsic chemical sensitivity, and domain composition cannot be determined without film destruction. Typically, AFM studies of binary or ternary polymer systems use either a complementary technique with chemical sensitivity (i.e., XPS, TOF-SIMS) or the selective removal of one component via washing with an appropriate solvent.[33−35] Thus, chemical characterization of these phase-segregated films required an additional technique, in this case X-PEEM.

The color-coded composite maps of the 40:60 and 60:40 PS:PLA ratio films derived from the X-PEEM C 1s data (Figure 4e−h) are a green color, indicating that for both ratios the surface is dominated by PLA. Although the AFM micrographs strongly suggested morphologies indicative of phase segregation, X-PEEM unambiguously reveals that there is a large excess of PLA in the near-surface region sampled (~10 nm) relative to the solution composition.

The spectra for the PS-rich and PLA-rich regions were extracted from the image sequences for 40:60 and 60:40 PS−PLA films using threshold masking,[36] and these spectra were then analyzed to quantify the composition of the discrete and continuous domains (Table 1). The PS region was compiled from the pixels with the most red color and is considered "PS-rich" relative to the PLA region. For the 40:60 PS:PLA ratio, the PLA-rich region has a composition of 86(5) vol % PLA and 14(5) vol % PS. In contrast, the PS-rich region consists of

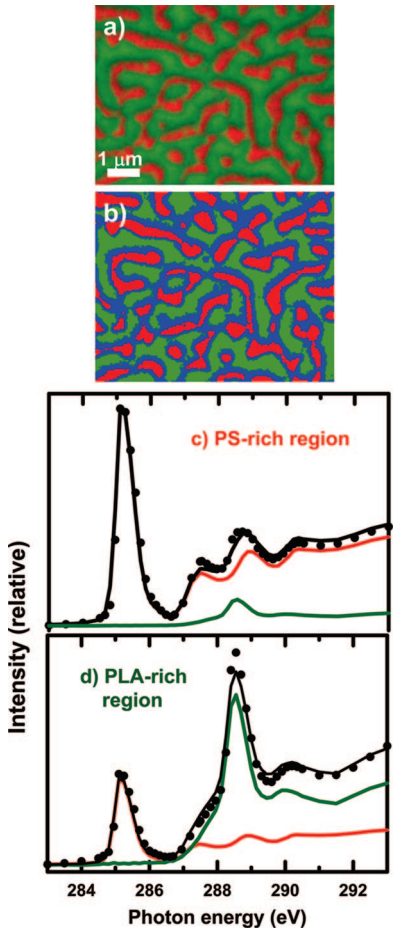

Figure 3. (a) Sample X-PEEM color-coded composite map (nonrescaled) derived from a singular value decomposition (SVD) analysis, using the PS and PLA reference spectra (Figure 1) of a C 1s image sequence (23 energies) recorded from a PS−PLA blend thin film spun-cast from a dichloromethane solution with a total loading of 0.7 wt % polymer in a 40:60 PS:PLA ratio, and annealed 6 h at 45 C. (b) Mask used to extract spectra of specific regions. Red denotes PS-rich regions, green denotes PLA-rich regions, defined by threshold masking the PS and PLA component maps. The remaining blue pixels represent areas with intermediate compositions which were not included in the quantitative analysis. (c) Curve fit of the average C 1s spectra of the PS-rich region (data, dots; fit, black line; components, colored lines). (d) Curve fit of the average C 1s spectra of the PLA-rich region (same color coding).

only 40(5) vol % PS with PLA contributing over 60(5) vol % of the signal. Analysis of the PS:PLA 60:40 blend shows even more anomalous results with an ∼80(5) vol % of PLA found in both the PS and PLA regions. The large percentage of PLA in the near surface region may indicate the presence of a relatively thick (∼8.0(5) nm) layer of PLA at the substrate surface.

PLA has also been found to segregate at the air−polymer interface in poly(sebacic anhydride) (PSA)−PLA blends.[37] In that case, the segregation was attributed to differences in the surface free energies of the polymer components, with the lower surface free energy polymer segregating to the surface.[37] However, the surface free energies of PS and PLA are very similar ($\gamma_{PLA} = 40.2$ mJ/m^2 and $\gamma_{PS} = 41.0$ mJ/m^2 [38,39]). Thus, it is more likely that the presence of excess PLA at the surface is due to the higher solubility of PLA in dichloromethane, such that the PLA stayed dissolved longer in the liquid phase and hence developed an overcoat layer.[40]

3.1.2. Total Polymer Concentration Dependence. The 40:60 PS:PLA composition was selected for dilution experiments since less PLA was detected in the X-PEEM study. The total percentage of polymer relative to the solvent was decreased from 1 to 0.7 wt % and then to 0.4 wt %, while maintaining the composition at the 40:60 ratio. AFM images (Figure 5a−c) show that the film cast from a 0.7 wt % solution exhibits a classic dispersed droplet morphology. Further dilution to 0.4 wt % produced a film with "blotchy" spots, likely corresponding to the same domains found for the 0.7 wt % film (Figure 5c).

The X-ray spectromicroscopy analysis of the 0.7 wt % PS:PLA 40:60 film reveals that phase segregation is incomplete. Although the PLA-rich region contains over 80(5) vol % PLA, PLA is also the dominant component in the PS region, contributing 60(5)% of the total signal (Figure 5d−f). In contrast, X-PEEM imaging of the 0.4 wt % 40:60 PS:PLA film shows a much more "red" color, corresponding to an increased signal from PS. The boundaries of the domains of PLA (green) are not sharp, which suggests that the PLA domains may be quite thin, as expected from the very dilute concentration of the polymer solution.

The 40:60 PS:PLA film showed negligible change in the PS fraction at the surface upon dilution from 1.0 to 0.7 wt % (Table 1). In fact, a fairly large fraction of PLA still exists in both the PS and PLA regions. In the PLA region, the PS fraction was 14(5)% in the 1.0 wt % to 19(5)% in the 0.7 wt % polymer solutions, which are the same values within experimental error. Upon further dilution of the solution to 0.4 wt %, the PS-rich regions now contain a stronger PS signal (75(5)%) while the PLA-rich region also shows a strong PS signal. Interestingly, the quantitative analysis of the three polymer concentrations (1, 0.7, and 0.4 wt %) indicates that the PS fraction increases upon dilution. One possible explanation may be that X-PEEM is detecting a layer of PS that exists under the PLA domains, leading to a more "red" color. Still, the quantitative X-PEEM results show that PS and PLA are not completely phase segregated.

3.1.3. Effect of Temperature. The morphology of a polymer blend can change significantly after annealing. For films with dispersed droplet structure, coarsening of the droplets is expected to occur from coalescence. Annealing also provides a means for driving the system toward its thermodynamic equilibrium, which in this case should be complete phase segregation of the PS and PLA. However, as we have annealed our films relatively gently it is likely that the observed changes in spatial distributions are primarily a result of kinetic factors. Typically, distributions in the unequilibrated as-coated system can be strongly affected by different solubilities or substrate affinities. These initial distributions can then be altered by annealing at temperatures in excess of the glass transition (T_g) temperature ($T_g \sim 60$ °C for PLA), where there is greater polymer mobility.[40] Samples of the 40:60 PS:PLA (0.7 wt %) film were annealed at 45 °C for 1 and 6 h and at 70 °C for 1 h. AFM micrographs of the annealed films demonstrate a progressive coarsening effect with increasing temperature, with the domains growing larger laterally and also in height (the surface corrugation increased from 35 nm in the unannealed film to 95 nm in the 70 °C annealed film) (Figure 6).

The X-PEEM results are consistent with the morphology determined by AFM. After annealing for 1 h at 45 °C, the PLA domains have begun to coalesce, which is further enhanced after annealing for 6 h. An additional 5 h of annealing at 45 °C led to further phase segregation of the two polymer components, with the green color of PLA becoming much more pure (Figure 6e). After annealing for 1 h at 70 °C, the domain size coarsens significantly and X-PEEM spectromicroscopy reveals that the discrete domains are now PS-rich (Figure 6f), as opposed to the as-cast and 45 °C annealed films in which the discrete domains are PLA-rich. Figure 2 compares the results from the

Table 1. Composition of PS and PLA (%/pixel) in the PS-Rich and PLA-Rich Regions of PS:PLA Blends with Respect to Polymer Ratios, Total Polymer Concentration, and Annealing (Uncertainty 5%)

		polymer ratios PS:PLA		conc dependence PS:PLA 40:60			annealing PS:PLA 40:60 (0.7%)		
region	component	40:60	60:40	1%	0.7%	0.4%	1 h at 45 °C	6 h at 45 °C	1 h at 70 °C
PS	PS	37	20	37	39	74	80	86	90
	PLA	63	80	63	61	26	20	14	10
PLA	PS	14	8	14	19	58	36	24	23
	PLA	86	92	86	81	42	64	76	77
film thickness[a] (±5 nm)		130	107	130	62	36	89	93	104

[a] Total film thickness (nm) as measured by AFM. Uncertainty estimated from repeat measurements over a scratch made with a sharp tweezer tip.

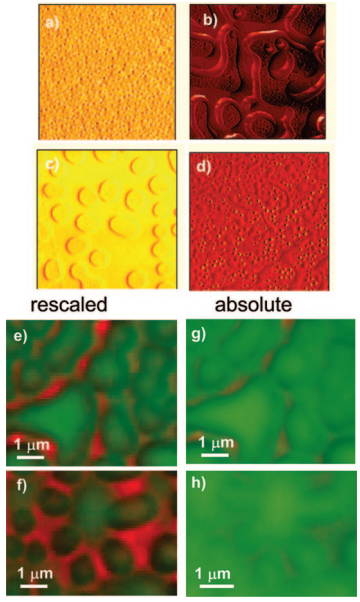

Figure 4. (upper four images) AFM phase mode images of PS:PLA thin film blends spun-cast from a 1 wt % dichloromethane solution loaded with PS:PLA in (a) 20:80 ratio, (b) 40:60 ratio, (c) 60:40 ratio, and (d) 80:20 ratio. All AFM images are 10 μm × 10 μm. (lower four images) X-PEEM color-coded composite map (rescaled) of (e) 40:60 PS:PLA ratio and (f) 60:40 PS:PLA ratio; the relative contribution from red has been increased 40%, and that of green has been decreased by 20% in order to visualize more clearly which is the continuous domain; (nonrescaled) of (g) PS:PLA 40:60 ratio and (h) PS:PLA 60:40 ratio. PS is coded red, and PLA is coded green.

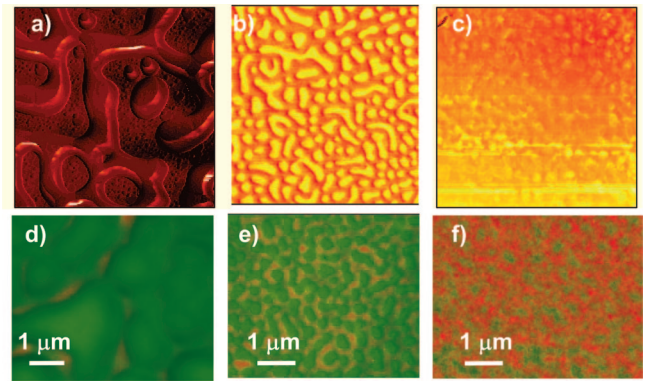

Figure 5. (upper row) AFM phase mode images of 40:60 PS:PLA films spun-cast from dichloromethane solutions with total polymer loading of (a) 1.0, (b) 0.7, and (c) 0.4 wt %. All AFM images are 10 μm × 10 μm. (lower row) X-PEEM color-coded composite maps (nonrescaled) of 40:60 PS:PLA films (d) 1.0, (e) 0.7, and (f) 0.4 wt %. PS is coded red, and PLA is coded green.

as-cast and most strongly annealed samples to emphasize this interesting phase-inversion result.

To verify the phase inversion indicated by X-PEEM, unannealed and 70 °C annealed PS−PLA films were washed with cyclohexane to selectively remove the PS component and re-examined with AFM (Figure 7). Analysis of the unannealed film after the wash showed very similar surface morphology compared to the unwashed film (Figure 7a,b). In contrast, AFM micrographs of cyclohexane-washed 70 °C annealed films (Figure 7c,d) revealed pitted circular holes consistent with the morphology and size of the discrete domains of PS prior to the cyclohexane wash. Thus, both X-PEEM and AFM of the solvent-modified sample consistently indicate that a phase inversion occurs when the as-cast films are annealed above the T_g of PLA.

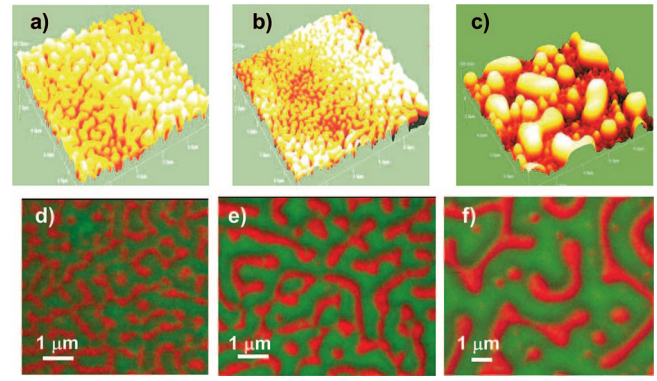

Figure 6. AFM height mode images of 40:60 PS:PLA thin films cast from a 0.7 wt % solution: (a) as-cast, maximum height 35 nm, (b) annealed 1 h at 45 °C, maximum height 45 nm, (c) annealed 1 h at 70 °C, maximum height 90 nm. All AFM images are 10 μm × 10 μm. X-PEEM color-coded composite maps (nonrescaled) of 40:60 PS:PLA thin films cast from a 0.7 wt % films which were (d) annealed 1 h at 45 °C, (e) annealed 6 h at 45 °C, and (f) annealed 1 h at 70 °C. PS is coded red, and PLA is coded green.

4. Discussion

Phase inversion caused by annealing has also been detected in PS−PMMA films spun-cast from toluene or THF. After annealing for 5 min above the T_g of both PS and PMMA (190 °C), a phase inversion was detected.[41] At present, we do not fully understand why the phase inversion in the PS−PLA thin film occurs below the T_g of PS. Phase inversion is known to be affected by volume fraction (ϕ) and structural parameters of the two polymers such as interfacial tension (σ), viscosity (η), and shear stress and strain (or elasticity).[42] In our case, the volume fraction remains unchanged, no shear stress is added, and the interfacial tensions of PS and PLA are very similar. We suggest that, although we are heating below the T_g of PS, there could be changes in the viscosity of the two polymers upon heating, leading to the phase inversion. This may be analogous to previously examined PMMA and poly(ethylene-*alt*-propylene) cryogenic mechanical alloying (CMA).[43] According to the Utracki model, adding one polymer to another polymer in either order causes an increase in the viscosity of the mixtures.[44] In order for a phase inversion to occur, the increasing viscosities must reach the same value. Thus, we speculate that by increasing our annealing temperature to 70

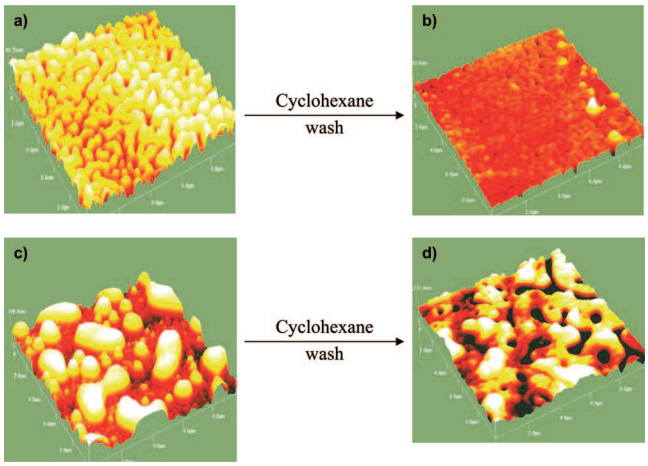

Figure 7. AFM height mode images of 40:60 PS:PLA thin films cast from a 0.7 wt % solution which were (a) as-cast, (b) as-cast, followed by wash with cyclohexane; (c) annealed 1 h at 70 °C, (d) annealed, followed by wash with cyclohexane. All images are 10 μm × 10 μm.

°C, the viscosities of PLA and PS may be similar enough to result in a phase inversion.

The quantitative X-PEEM analyses show there is a considerable increase in the degree of phase separation with annealing, as indicated by greater purity of the discrete and continuous domains. Further enhancement is seen with longer annealing time, especially in the PLA-rich region. However, although higher temperature dramatically impacts the morphology, it does not result in complete phase segregation (Table 1). In the PS-rich region there still remains ∼10% of PLA, while in the PLA-rich region there is 20−30% of PS.

For complete phase segregation, annealing at temperatures in excess of the T_gs of both PS and PLA is required. For example, in the case of PS−PMMA thin films which were annealed at 142 °C for 42 h and 170 °C for 8 days, it was found that the morphology obtained at the lower temperature was a transient state which only approached equilibrium upon annealing at higher temperature.[45] In the case of PS−PLA, annealing at a temperature of ∼170 °C is impossible due to the low melting point (T_m) of PLA, which is 145−200 °C depending on MW and 145 °C at a MW of 33 000 g/mol.[46−48] Clearly, our PS−PLA films are not fully equilibrated. Yet, even in the case of PS−PMMA, annealing for 8 days at 170 °C did not result in a fully equilibrated sample.[45] Furthermore, since the surface tensions of PS and PLA are very similar, the calculated parameters controlling PS spreading on PLA ($S_{PS} = \gamma_{PLA} - \gamma_{PS} - \gamma_{PS/PLA}$) and vice versa ($S_{PLA} = \gamma_{PS} - \gamma_{PLA} - \gamma_{PS/PLA}$) are both negative, meaning neither polymer can wet the other.[45] Thus, if the sample is thermally equilibrated, PS and PLA should be fully phase segregated in both the bulk and at the surface.[45]

Literature reports of bulk PS−PLA blends examined by differential scanning calorimetry (DSC) and thermal gravimetric analysis (TGA) reveal that the miscibility of the two polymers is highly dependent on polymer composition, with some data sets showing miscibility while others suggesting immiscibility.[10] A Fourier transform infrared photoacoustic spectroscopy (FTIR-PAS) study has detected the formation of n−π bonds between the carboxyl groups of PLA and the benzyl rings of PS, possibly contributing to the incomplete phase segregation.[10] Nonetheless, it is much more likely that small trapped microdomains of the opposite polymer exist at or below the spatial resolution of the X-PEEM, hence giving rise to measurable amounts of the minority component in the quantitative analysis. The existence of small microdomains is evident in the PLA region in the AFM micrographs (Figure 6c).

5. Conclusions

The chemical purity of domains at the surface of a partially phase-segregated PS−PLA blend has been optimized by investigating the morphological and chemical dependence of the thin films with respect to polymer ratio, total polymer concentration, and annealing protocol (time and temperature). While annealing at 70 °C gave a significant improvement in the extent of phase segregation, further optimization of the annealing process is needed in order to achieve 100% phase segregation and eliminate the microdomains. Interestingly, a phase inversion was seen when the films were annealed at temperatures above the T_g of PLA. We interpret this as the result of thermal evolution of the viscosity. Our X-PEEM results show that, in this case, the surface composition suggested by AFM did not correspond to the actual chemical composition, emphasizing the value of an independent verification by a chemically sensitive analysis such as XPEEM or by chemically removing one component from the system.

The annealed PS−PLA blends exhibit a structured surface morphology with distinct surface energies and functional groups. This is required for preferential domain interactions with specific biomacromolecules, a property which might be desired for certain biomaterials applications. In a companion publication we will report our X-PEEM studies of preferential protein adsorption on the best chemically segregated PS−PLA surface.

Acknowledgment. This research is supported by the Natural Science and Engineering Research Council (NSERC, Canada) and the Canada Research Chair programs. X-ray microscopy was carried out using PEEM2 and the polymer STXM at the ALS which is supported by the US Department of Energy under Contract DE-AC03-76SF00098.

References and Notes

(1) Ragauskas, A. J.; Williams, C. K.; Davison, B. H.; Britovsek, G.; Cairney, J.; Eckert, C. A.; Frederick, W. J.; Hallet, J. P.; Leak, D. J.; Liotta, C. L.; Mielenz, J. R.; Murphy, R.; Templer, R.; Tschaplinski, T. *Science* **2006**, *311*, 484–489.
(2) Athanasiou, K. A.; Niederauer, G. G.; Agrawal, C. M. *Biomaterials* **1996**, *17*, 93–102.
(3) Hutmacher, D. W. *Biomaterials* **2000**, *21*, 2529–2543.
(4) Bhardwaj, R.; Mohanty, A. K. *Biomacromolecules* **2007**, *8*, 2476–2484.
(5) Willet, J. L.; Shogren, R. L. *Polymer* **2002**, *43*, 5935–5947.
(6) Li, J.; He, Y.; Inoue, Y. *Polym. Int.* **2003**, *52*, 949–955.
(7) Ljungberg, N.; Wesslen, B. *Polymer* **2003**, *44*, 7679–7688.
(8) Ljungberg, N.; Wesslen, B. *Biomacromolecules* **2005**, *6*, 1789–1796.
(9) Frick, E. M.; Zalusky, A. S.; Hillmyer, M. A. *Biomacromolecules* **2003**, *4*, 216–223.
(10) Mohamed, A.; Gordon, S. H.; Biresaw, G. *J. Appl. Polym. Sci.* **2007**, *106*, 1689–1696.
(11) Olayo-Valles, R.; Lund, M. S.; Leighton, C.; Hillmyer, M. A. *J. Mater. Chem.* **2004**, *14*, 2729–2731.
(12) Zalusky, A. S.; Olayo-Valles, R.; Wolf, J. H.; Hillmyer, M. A. *J. Am. Chem. Soc.* **2002**, *124*, 12761–12773.
(13) Ho, R. M.; Tseng, W. H.; Fan, H. W.; Chiang, Y. W.; Lin, C. C.; Ko, B. T.; Huang, B. H. *Polymer* **2005**, *46*, 9362–9377.
(14) Sarazin, P.; Favis, B. D. *Biomacromolecules* **2003**, *4*, 1669–1679.
(15) Bates, F. S.; Fredrickson, G. H. *Annu. Rev. Phys. Chem.* **1990**, *41*, 525–557.
(16) Slep, D.; Asselta, J.; Rafailovich, M. H.; Sokolov, J.; Winesett, D. A.; Smith, A. P.; Ade, H.; Anders, S. *Langmuir* **2000**, *16*, 2369–2375.
(17) Si, M.; Araki, T.; Ade, H.; Kilcoyne, A. L. D.; Fisher, R.; Sokolov, J. C.; Rafailovich, M. H. *Macromolecules* **2006**, *39*, 4793–4801.
(18) Tzvetkov, G.; Graf, B.; Wiegner, R.; Raabe, J.; Quitmann, C.; Fink, R. *Micron* **2008**, *39*, 275–279.
(19) Hitchcock, A. P.; Stöver, H. D. H.; Croll, L. M.; Childs, R. F. *Aust. J. Chem.* **2005**, *58*, 423–432.
(20) Zhu, S.; Liu, Y.; Rafailovich, M. H.; Sokolov, J.; Gersappe, D.; Winesett, D. A.; Ade, H. *Nature (London)* **1999**, *400*, 49–51.
(21) Ade, H.; Winesett, D. A.; Smith, A. P.; Qu, S.; Ge, S.; Sokolov, J.; Rafailovich, M. *Europhys. Lett.* **1999**, *45*, 526–532.
(22) Morin, C.; Ikeura-Sekiguchi, H.; Tyliszczak, T.; Cornelius, R.; Brash, J. L.; Hitchcock, A. P.; Scholl, A.; Nolting, F.; Appel, G.; Winesett,

D. A.; Kaznacheyev, K.; Ade, H. *J. Electron Spectrosc. Relat. Phenom.* **2001**, *121*, 203–224.
(23) Leung, B. O.; Hitchcock, A. P.; Brash, J. L.; Scholl, A.; Doran, A. Manuscript in preparation.
(24) Warwick, T.; Ade, H.; Kilcoyne, A. L. D.; Kritscher, M.; Tylisczcak, T.; Fakra, S.; Hitchcock, A. P.; Hitchcock, P.; Padmore, A. H. *J. Synchrotron Radiat.* **2002**, *9*, 254–257.
(25) Kilcoyne, A. L. D.; Tylisczak, T.; Steele, W. F.; Fakra, S.; Hitchcock, P.; Franck, K.; Anderson, E.; Harteneck, B.; Rightor, E. G.; Mitchell, G. E.; Hitchcock, A. P.; Yang, L.; Warwick, T.; Ade, H. *J. Synchrotron Radiat.* **2003**, *10*, 125–136.
(26) Jacobsen, C. J.; Zimba, C.; Flynn, G.; Wirick, S. *J. Microsc.* **2000**, *19*, 173–184.
(27) Wang, J. Ph.D Thesis, Department of Chemistry, McMaster University, Hamilton, Ontario, Canada, **2008**.
(28) Anders, S.; Padmore, H. A.; Duarte, R. M.; Renner, T.; Stammler, T.; Scholl, A.; Scheinfein, M. R.; Stohr, J.; Seve, L.; Sinkovic, B. *Rev. Sci. Instrum.* **1999**, *70*, 3973–3981.
(29) Wang, J.; Li, L.; Morin, C.; Hitchcock, A. P.; Doran, A.; Scholl, A. *J. Electron Spectrosc.* **2009**, doi: 10.1016/j.elspec.2008.01.002.
(30) aXis 2000 is free for noncommercial use. It is written in Interactive Data Language (IDL) and available from http://unicorn.mcmaster.ca/aXis2000.html.
(31) Strang, G. *Linear Algebra and Its Applications*; Harcourt Bracourt, Jovanovich: San Diego, 1988.
(32) Koprinarov, I. N.; Hitchcock, A. P.; McCrory, C. T.; Childs, R. F. *J. Phys. Chem. B* **2002**, *106*, 5358–5364.
(33) Wang, P.; Koberstein, J. T. *Macromolecules* **2004**, *37*, 5671–5681.
(34) Walheim, S.; Ramstein, M.; Steiner, U. *Langmuir* **1999**, *15*, 4828–4836.
(35) Virgilio, N.; Favis, B. D.; Pepin, M.-F.; Desjardins, P.; L'Esperance, G. *Macromolecules* **2005**, *38*, 2368–2375.
(36) L.Li, L.; Brash, J.; Cornelius, R.; and Hitchcock, A. P. *J. Phys. Chem. B* **2008**, *112*, 2150–2158.
(37) Davies, M. C.; Shakesheff, K. M.; Shard, A. G.; Domb, A.; Roberts, C. J.; Tendler, S. J. B.; Williams, P. M. *Macromolecules* **1996**, *29*, 2205–2212.
(38) Ton-That, C.; Shard, A. G.; Teare, D. O. H.; Bradley, R. H. *Polymer* **2001**, *42*, 1121–1129.
(39) Otsuka, H.; Nagasaki, Y.; Kataoka, K. *Sci. Technol. Adv. Mater.* **2000**, *1*, 21–29.
(40) Ton-That, C.; Shard, A. G.; Daley, R.; Bradley, R. H. *Macromolecules* **2000**, *33*, 8453–8459.
(41) Walheim, S.; Boltau, M.; Mlynek, J.; Krausch, G.; Steiner, U. *Macromolecules* **1997**, *30*, 1995–5003.
(42) Steinmann, S.; Gronski, W.; Friedrich, C. *Polymer* **2001**, *42*, 6619–6629.
(43) Smith, A. P.; Ade, H.; Smith, S. D.; Koch, C. C.; Spontak, R. J. *Macromolecules* **2001**, *34*, 1536–1538.
(44) Utracki, L. A. *J. Rheol.* **1991**, *35*, 1615–1637.
(45) Haris, M.; Appel, G.; Ade, H. *Macromolecules* **2003**, *36*, 3307–3314.
(46) Woo, S. I.; Kim, B. O.; Jun, H. S.; Chang, H. N. *Polym. Bull.* **1995**, *35*, 415–421.
(47) Chen, C. C.; Chueh, J. Y.; Tseng, H.; Huang, H. M.; Lee, S. Y. *Biomaterials* **2003**, *24*, 1167–1173.
(48) Ajioka, M.; Enomoto, K.; Suzuki, K.; Yamaguchi, A. *J. Environ. Polym. Degrad.* **1995**, *3*, 225–234.

MA802176B